



# Assessment of flood mitigation through riparian detention in response to a changing climate – a case study

KWAN TUN LEE and PIN-CHUN HUANG\*

*Center of Excellence for Ocean Engineering, National Taiwan Ocean University, Keelung, Taiwan.*

*\*Corresponding author. e-mail: pinchunhuang@gmail.com*

MS received 7 February 2017; revised 1 November 2017; accepted 20 December 2017;  
published online 2 August 2018

Considering that urban areas may suffer more substantial losses than riparian farmlands during floods, diverting floodwater into riparian areas for temporal detention is expected to mitigate flood damage in downstream urban areas. In this study, an assessment has been conducted to evaluate the effect of flood mitigation through riparian detention in response to a changing climate in the Tou-Chien River basin of Taiwan. An integrated 1D–2D flow model was used to simulate the movement of flood wave in the main stream and the overbank flow inundating into the nearby lowlands. Based on the numerical simulation results, the flooding extents in the basin corresponding to different return periods of flood using existing flood prevention infrastructures were investigated. A detention strategy by lowering the levee along the riparian farmlands was proposed to avoid severe flooding in the densely populated urban areas of the basin. Research findings showed that the proposed detention measure can completely protect the downstream areas from overbank flooding when a flood having 20-yr period occurs, and can effectively alleviate the downstream flooding area from 27.4 to 7.6 km<sup>2</sup> for a flood possessing 200-yr period.

**Keywords.** Flood detention; urban flooding; channel-flow routing; overland-flow routing; overbank flow.

## 1. Introduction

According to the analysis results announced by the [World Bank \(2005\)](#), Taiwan has been recognized as the most vulnerable region in respect of natural disasters. In the main island of Taiwan, approximately 73% of residents are threatened by three different types of natural hazards, in which the flood disaster occurs most frequently. As revealed by hourly precipitation data from 21 gauging stations in northern Taiwan, the amount of extreme rainfall was found to increase significantly from 1994 to 2011 ([Su et al. 2012](#)). Reassessing the criteria of levee height for flood protection is therefore a routine work that cannot be ignored. The design of levee crest usually depends on the results

of frequency analysis using hydrological records; hence, it can be inferred that the standard of levee height for flood protection would be altered as available hydrological data are extended. Although levee heightening is one of the most straightforward strategies that can be implemented by authorities, it may not be practically feasible due to a variety of constraints, such as bridge and road reconstruction, land-use planning, landscape considerations, and fiscal budgets. Considering that urban areas may receive more disastrous damage than agricultural fields during floods, diverting part of the flood water from the upstream main channel to riparian farmlands for flood peak attenuation could be a compromising measure to alleviate downstream urban flooding.

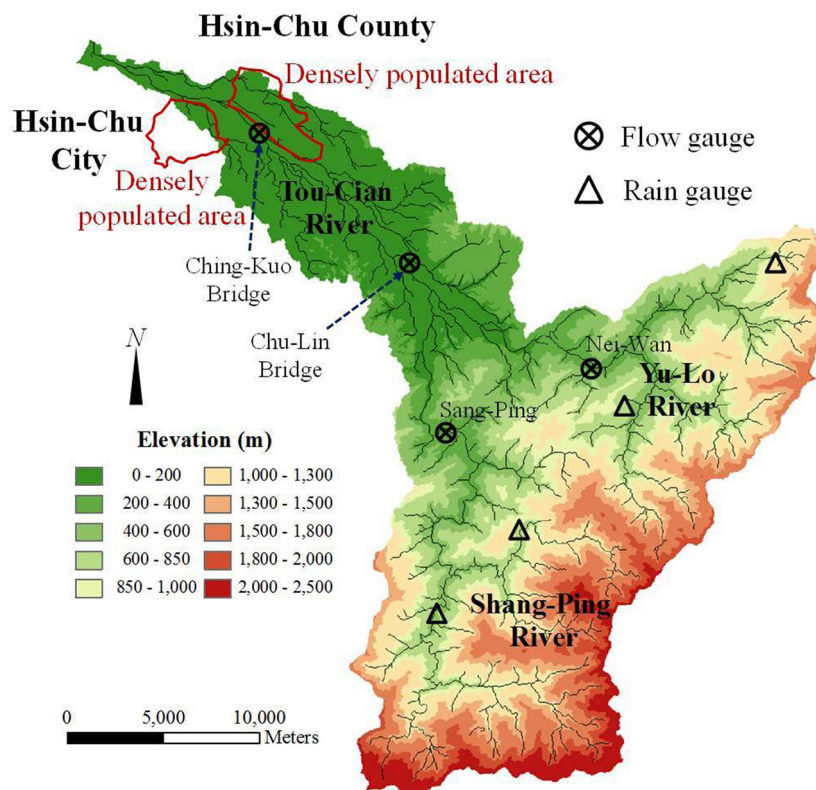


Figure 1. Geographical location and topography of the Tou-Chien River basin.

To investigate the effect of flood mitigation through riparian detention, modeling different possible strategies to divert the flood water can be conducted by using numerical models. In order to execute the hydrological simulations, this study establishes an integrated 1D–2D model, which combines a one-dimensional channel-flow routing with a two-dimensional overland-flow routing. For the channel-flow simulation, a four-point implicit Preissmann scheme (Preissmann 1961) was employed to solve the fully dynamic-wave equation. The diffusion-wave approximation was then applied for the overland-flow simulation, because it was proved to provide appropriate simplification for rainfall-runoff routing and accommodate complicated land surfaces (Ponce *et al.* 1978; Gonwa and Kavvas 1986; Ogden and Julien 1993; Wang and Hjelmfet 1998; Jain and Singh 2005). Moreover, the exchange of floodwater between channel and overland area was achieved by using weir equations to evaluate the volume of overbank discharge (Cunge *et al.* 1980; Pasche and Rouvé 1985; Hager 1987; Nicholas and Walling 1997).

The main objective of this paper is to assess the efficacy of flood mitigation in the downstream urban areas through riparian farmlands detention

in the Tou-Chien River basin. In the following sections of this paper, climate variability in the basin is firstly investigated through trend identification and frequency analysis based on available discharge records. The 1D–2D numerical model is subsequently implemented to investigate the spatial distributions of the inundated water depth corresponding to different return periods of flood. A detention strategy through lowering the levees near the predetermined riparian farmlands was conducted to evaluate the flood peak attenuation in the downstream urban areas. The strategy is promising to be adopted by authorities to alleviate flooding in the urban areas of Tou-Chien River basin.

## 2. Study area

The geographical location and topography of the Tou-Chien River basin located in northwest Taiwan is shown in figure 1. The watershed area is about 566 km<sup>2</sup> and is administrated by Hsinchu County and Hsinchu City. The average slope of the basin is 0.0053, and the total length of the main stream is 63.06 km. There are two major upstream

tributaries contributing to the Tou-Chien River, in which the Yu-Lo River is about 26 km long with an average slope of 0.021 and the Shang-Ping River is about 44 km long with an average slope of 0.020. There are four rain-gauging stations in the basin providing continuous hourly precipitation data. The average annual rainfall measured at the Hsinchu Station is 1747 mm. The rainfall in the basin shows an uneven distribution with time and space as a result of the periodical southwest monsoon and typhoons. The wet season is occurred in the period from June to September. Figure 1 also shows the locations of four existing flow-gauging stations. The Nei-Wan and Shang-Ping Stations are located on the Yu-Lo and Shang-Ping tributaries, respectively; and the other two flow stations, the Chu-Lin Bridge and Ching-Kuo Bridge, are installed at the mainstream of Tou-Chien River.

As shown in figure 1, two densely populated urban areas (marked with red line) are distributed along the downstream of the Tou-Chien River. The left side of the river governed by Hsinchu City is occupied by many commercial buildings with dense population. The Hsinchu Science Park is located at the right side of the river, which has stimulated a rapid development of the Hsinchu County in recent years. The Park is the first and the most important place to develop semiconductor and photovoltaics technologies in Taiwan, has created an annual output value of more than 40 billion US dollars and attracted a large number of domestic and international investments. The impressive revenue leads the Park to be referred to as Taiwan's Silicon Valley. Consequently, flood prevention in the downstream areas of Tou-Chien River is one of the most important works for regional authorities.

According to the report published by the Water Resources Planning Institute (2011), most of the levees along the Tou-Chien River were built before 1992; hence, the levee-crest elevation in this basin was designed according to the result of frequency analysis using flow record data before 1992. As more frequent and severe rainstorms have been observed in Taiwan in recent years, a concern was raised about that whether the levee-crest design based on the previous frequency analysis results using early recorded data could meet current flood prevention criterion. To answer this question, statistical analysis should be employed to realize the variability of the hydrological process in the Tou-Chien River basin.

## 2.1 Climate variability detection

Although the most widely used method for trend identification is the Mann–Kendall test (Mann 1945; Kendall 1975), the method is restricted by several conditions, such as the independent time series without any serial correlation, the normality of the data distribution, and the required data length (Sen 2012). Moreover, the Mann–Kendall test is incapable to indicate the magnitude of trend for a given data series. To conquer the aforementioned restrictions, an innovative analysis proposed by Sen (2012) was adopted in this study. The basis of this approach is to compare the later period of time series with the early one in order to detect the tendency that is inherent in a time series data. Therefore, the series data has to be divided into two half portions firstly; then the analysis method can be performed by plotting them in ascending order on a Cartesian coordinate system. As reported by the reference paper (Sen 2012), if the data points distribute mainly along the 45° straight line in the plot, it implies a trend-free time series; on the contrary, if the data points lie above (or below) the 45° straight line, it implies a monotonic increasing (or decreasing) trend. It should be noted that there is another situation that data points scatter on both sides of the 45° line significantly, which corresponds to the non-monotonic trend having both the increasing and decreasing tendencies simultaneously at different scales of time series.

Annual-maximum discharge records from 1976 to 2011 at Nei-Wan station, Shang-Ping station, and Chu-Lin Bridge station were collected for analysis. The downstream Ching-Kuo Bridge Station was not included in the trend analysis because the record before 1990 was unavailable. The available records of annual-maximum streamflow were separated into two periods. The first data series for the trend analysis ranges from 1976 to 1993, and the second series ranges from 1994 to 2011. This separation of data periods referred to the significant change of extreme rainfall observed in 1994–2011, which was indicated by Su *et al.* (2012). The analysis results are shown in figure 2, in which the x-axis is the data series from 1976 to 1993; and the y-axis is the data series from 1994 to 2011. Both of the data series for each station were sorted in ascending order and then plotted on the graph. Figure 2(a) shows that most of the data points fall above the 45° line, which demonstrates that the discharge observed at the Nei-Wan Station has an increasing trend. In figure 2(b), the

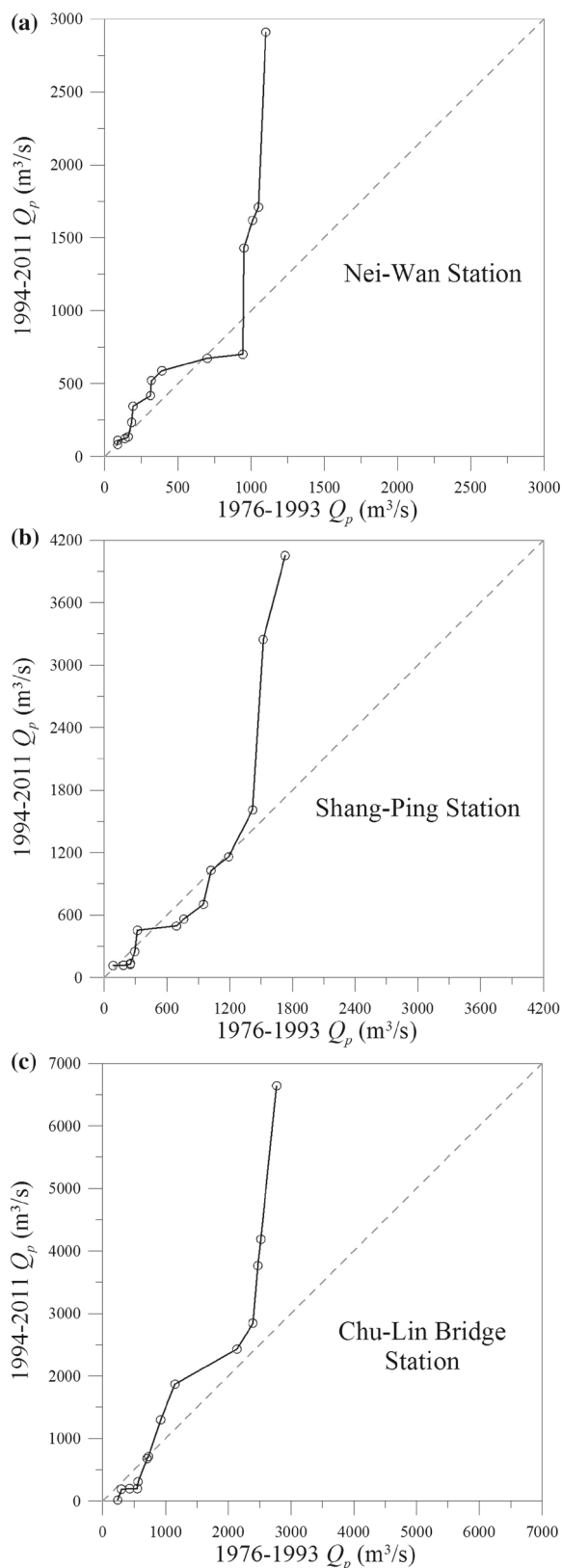


Figure 2. Trend analyses of the annual maximum discharge series for the Nei-Wan, Shang-Ping, and Chu-Lin Bridge stations. (a) Nei-Wan station, (b) Shang-Ping station, and (c) Chu-Lin Bridge station.

streamflow data monitored at the Shang-Ping Station reveals a non-monotonic trend in the given period because the scatter of points spread on both sides of the 45° line. Nevertheless, the high-flow data points lie above the 45° line and present an increasing trend. A similar situation can be seen in figure 2(c) for the Chu-Lin Bridge Station. The results have confirmed an increasing trend of the high-flow data from 1994 to 2011 in comparison with the data series of 1976–1993, especially for the record observed at the Chu-Lin Bridge Station which is located at the main stream of the Tou-Chien River.

Five probability distributions, two-parameter lognormal, three-parameter lognormal, Pearson type III, log-Pearson type III, and extreme value type I, were adopted for frequency analysis. The Chi-square test and Kolmogorov–Smirnov test based on a confidence level of 95% were implemented to examine the acceptability of the probability distribution assumptions. The available records of annual maximum discharge from 1976 to 2011 were grouped into two segments of data series for analysis. The results of the frequency analysis applying different periods of data are shown in table 1, in which Pearson type III distribution was adopted considering its minimum standard error among the five probability distributions. For the two upstream stations (Nei-Wan and Shang-Ping), flood peaks derived from the data period of 1976–2011 for different return periods are larger than those acquired from the data period of 1976–1993. More significant increase of the flood peaks can be found in the downstream main channel by analyzing the data of Chu-Lin Bridge Station. Since the existing levees along the mainstream of Tou-Chien River were built before 1992, the increased flood risk induced by the changing climate in the basin can be inferred.

### 3. Numerical modelling

An integrated numerical model was developed in this study for flooding simulation to realize the flood risk resulting from the changing climate and to propose possible strategies for flooding mitigation. The integrated 1D–2D numerical model contains an overbank flow routing module, a channel-flow routing module, and a mechanism for determining the overbank discharge.

Table 1. Frequency analysis results for annual peak discharge using different periods of records.

Station	Data period	Mean of annual peak discharge (cm)	Peak discharge for different return periods (cm)				
			10-yr	20-yr	50-yr	100-yr	200-yr
Nei-Wan	1976–1993	1276.1	971	1249	1657	2002	2379
	1976–2011	1669.7	1443	1848	2407	2853	3319
Shang-Ping	1976–1993	1276.1	1827	2232	2755	3147	3537
	1976–2011	1669.7	2324	2922	3695	4274	4851
Chu-Lin Bridge	1976–1993	1276.1	2530	2967	3493	3866	4223
	1976–2011	1669.7	3797	4810	6175	7241	8341

Note: Peak discharge for different return periods were estimated by Pearson type III distribution.

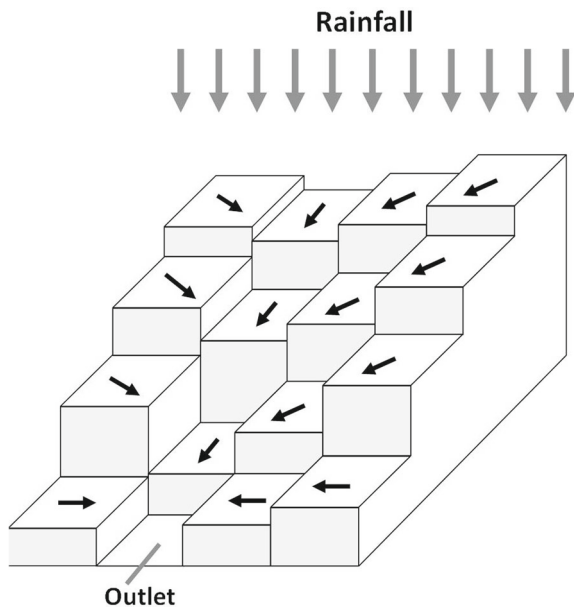


Figure 3. Schematic diagram of the flow-direction determination for overland-flow routing.

### 3.1 Overland-flow routing

As shown in figure 3, the single flow direction of each cell is applied for the grid-based overland-flow routing following the eight-direction (D8) algorithm (O’Callaghan and Mark 1984), in which the water mass has to be appointed from one cell to the adjacent cell having the steepest descent of water stage. Therefore, the expression of the governing equation is essentially in the 1D (or quasi-2D) form. The continuity equation for overland-flow simulation can be written as:

$$\frac{\partial y}{\partial t} + \frac{\partial (V_o y)}{\partial x} = i_e, \quad (1)$$

where  $y$  is the overland-flow depth;  $i_e$  is the rainfall excess rate; and  $V_o$  is the overland-flow velocity

which can be estimated by

$$V_o = \frac{1}{n} y^{2/3} S_f^{1/2}, \quad (2)$$

where  $n$  is the Manning’s roughness coefficient and  $S_f$  is the friction slope. The simplified momentum equation based on the diffusion-wave approximation can be expressed as:

$$S_f = S_o - \frac{\partial y}{\partial x} \quad (3)$$

where  $S_o$  is the ground slope. An explicit MacCormack scheme (MacCormack 1982; Huang and Lee 2013, 2017) was adopted to solve the governing equations. It has been indicated that this numerical scheme can be adequately and efficiently applied for simulating surface runoff on a raster-based elevation dataset (Wang and Hjelmfet 1998; Léonard et al. 2004; Pantelakis et al. 2012; Huang and Lee 2013, 2017).

### 3.2 Channel-flow routing

The one-dimensional Saint-Venant equations are usually used to simulate unsteady open channel flow. The continuity equation for channel-flow routing can be expressed as:

$$\frac{\partial A}{\partial t} + \frac{\partial Q}{\partial x} = q_l \quad (4)$$

in which  $A$  is the cross-sectional area of channel flow;  $Q$  is the flow discharge; and  $q_l$  is the lateral flow. A positive  $q_l$  represents the lateral inflow draining from overland area into channel; whereas a negative  $q_l$  corresponds to the part of channel flow overflowing to riparian areas. A one-dimensional dynamic-wave equation, considering complete force

terms, can be written as:

$$\frac{\partial Q}{\partial t} + \frac{\partial(\beta QV)}{\partial x} + gA \frac{\partial y}{\partial x} = gA(S_c - S_f) + \beta q_l V_{lx} \quad (5)$$

in which  $\beta$  is the momentum coefficient;  $g$  is the acceleration due to gravity;  $S_c$  is the channel bed slope;  $V$  is the channel-flow velocity, and  $V_{lx}$  is the velocity component of the lateral flow in the main-stream direction. A four-point implicit finite-difference scheme (Preissmann 1961) was implemented to discrete equations (4 and 5). The channel-flow routing then can be performed to imitate the phenomena of flood wave propagation if initial and boundary conditions are prescribed properly.

### 3.3 Overbank-flow determination

Overbank-flow calculation can be broadly categorized into two situations based on the flow patterns of submerged or free overflow. The exchange of floodwater between the channel and overland grids, either channel flow inundating to the riparian areas or overland flow draining into the channel, can be determined by using following equations (Cunge *et al.* 1980):

$$Q = C_1 \sqrt{2g} \cdot B (y_{ds} - y_w) (y_{us} - y_{ds})^{1/2} \quad (6)$$

$$Q = C_2 \sqrt{2g} \cdot B (y_{us} - y_w)^{3/2} \quad (7)$$

in which  $y_{us}$  is the water surface elevation on the upstream side of the levee crest;  $y_{ds}$  is the water surface elevation on the downstream side of the levee crest;  $B$  is the length of the levee;  $y_w$  is the levee crest elevation;  $C_1$  and  $C_2$  are discharge coefficients. Equation (6) is used to simulate the overbank flow analogous to a drowned weir; and equation (7) is used to simulate the overbank flow in a free-overflow situation. Figure 4 is a schematic diagram showing the flow connection between the channel and overland area in the proposed numerical model. The volume of overbank flow through one side of levee along a channel reach is uniformly distributed to the adjacent overland cells (for instance, the No: 1, 2, 3 and 4 cells shown in figure 4) when the water stage of a channel reach is higher than any side of the levee crest. On the contrary, surface flow on the overland cells along the both sides of channel

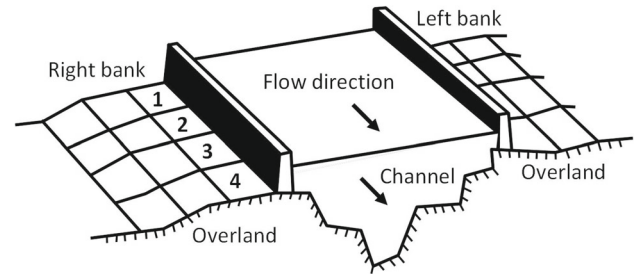


Figure 4. Schematic diagram of a channel reach connecting to its floodplain cells.

would drain into the nearest channel reach if the overland-flow stage is higher than the channel-flow stage.

## 4. Model application and discussion

There are two primary issues to be addressed in this section by a series of numerical simulations. First, the assessment is made on the extent of flooding in the densely populated urban areas induced by the changing climate under the situation of existing levees along the main stream of Tou-Chien River. Second, the performance of the riparian detention for downstream inundation mitigation is evaluated. Although digital elevation datasets have been widely linked with numerical methods for runoff simulations, the grid-based model usually requires more time for computation. In order to enhance the computational efficiency, only the downstream flat areas, more prone to flooding, are considered in executing the integrated 1D–2D flow model for flow analysis. Moreover, the horizontal resolution of the elevation dataset (cell size) adopted in the proposed model is 40 m; and the dataset format is orthogonal raster. Figure 5 shows the region for flooding simulation using the 1D–2D model, in which the densely populated urban areas are marked out with red lines and the riparian farmlands for flood detention are marked out with green lines. In the following paragraphs, the model parameter determination, the analysis of flooding extent, and the assessment of riparian detention will be discussed accordingly.

### 4.1 Model parameters determination

The general ranges of land surface roughness suggested by the Hydrologic Engineering Center (HEC

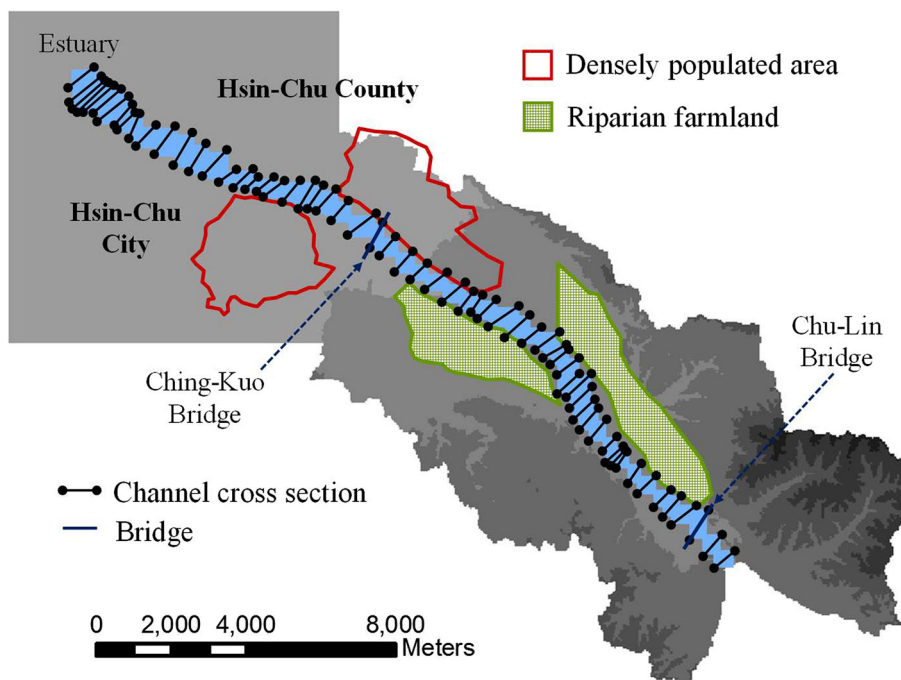


Figure 5. Inundation simulation region in the Tou-Chien River basin.

2000) according to various land-cover conditions were referred in this study. Subsequently, flow records at Chu-Lin Bridge and Ching-Kuo Bridge were then collected to calibrate the optimal values of Manning’s roughness coefficients by conducting a series of runoff simulations, assigned with different storm events. Through the calibration process to adjust the model parameters, it can be determined that the roughness coefficients assigned to the channel reaches were in the range of 0.028–0.035 for the 1D channel-flow routing. As regards the 2D overland-flow routing, since the inundation records are currently unavailable, the table indicating the surface roughness (HEC 2000) is the basis of reference considered in this study. Basically, the roughness coefficients are 0.1 for building and road, 0.25 for bare soil, 0.35 for pasture, and 0.65 for woods. Figure 6 shows the flood event brought by Typhoon Doug, occurred on 7 August, 1994. The discharge hydrograph measured at Chu-Lin Bridge, as shown in figure 6(a), was used as the upstream boundary condition for the 1D channel-flow routing; and the tide record collected from the Nan-Liao harbor at the river mouth of the Tou-Chien River was adopted as downstream boundary condition. The simulated flow hydrograph shown in figure 6(b) demonstrates that the 1D dynamic-wave model is capable of providing reliable channel-flow simulation by adopting the optimal magnitudes of Manning’s roughness coefficient.

#### 4.2 Flooding extent analysis

To realize the extent of flooding in the densely populated urban areas induced by the changing climate, series of numerical tests were conducted under the situation of existing levees along the mainstream of Tou-Chien River. In this study, to avoid using conventional triangular hydrographs, the observed hydrograph shown in figure 6(a) for Typhoon Doug was treated as the basic shape to generate design inflow hydrographs. As shown in figure 7, the peak discharges of the design hydrographs correspond to the results of the frequency analysis at Chu-Lin Bridge Station (as shown in table 1) based on the recorded data from 1977 to 2011, and the shape of the design hydrographs is linearly proportional to the flow hydrograph measured at the Chu-Lin Bridge during Typhoon Doug. Extreme tide levels corresponding to different return periods at the estuary of Tou-Chien River (Water Resources Planning Institute 2011) were used as the downstream boundary conditions for the dynamic-wave channel routing.

Figure 8 shows the existing levee crest (black line), the channel bed profile (brown line), and the computed water-stage profile corresponding to the 10-yr return-period flood (blue line). It is noted that the existing levee crest in several channel reaches is lower than the 10-yr water stage, although the original design of embankment was

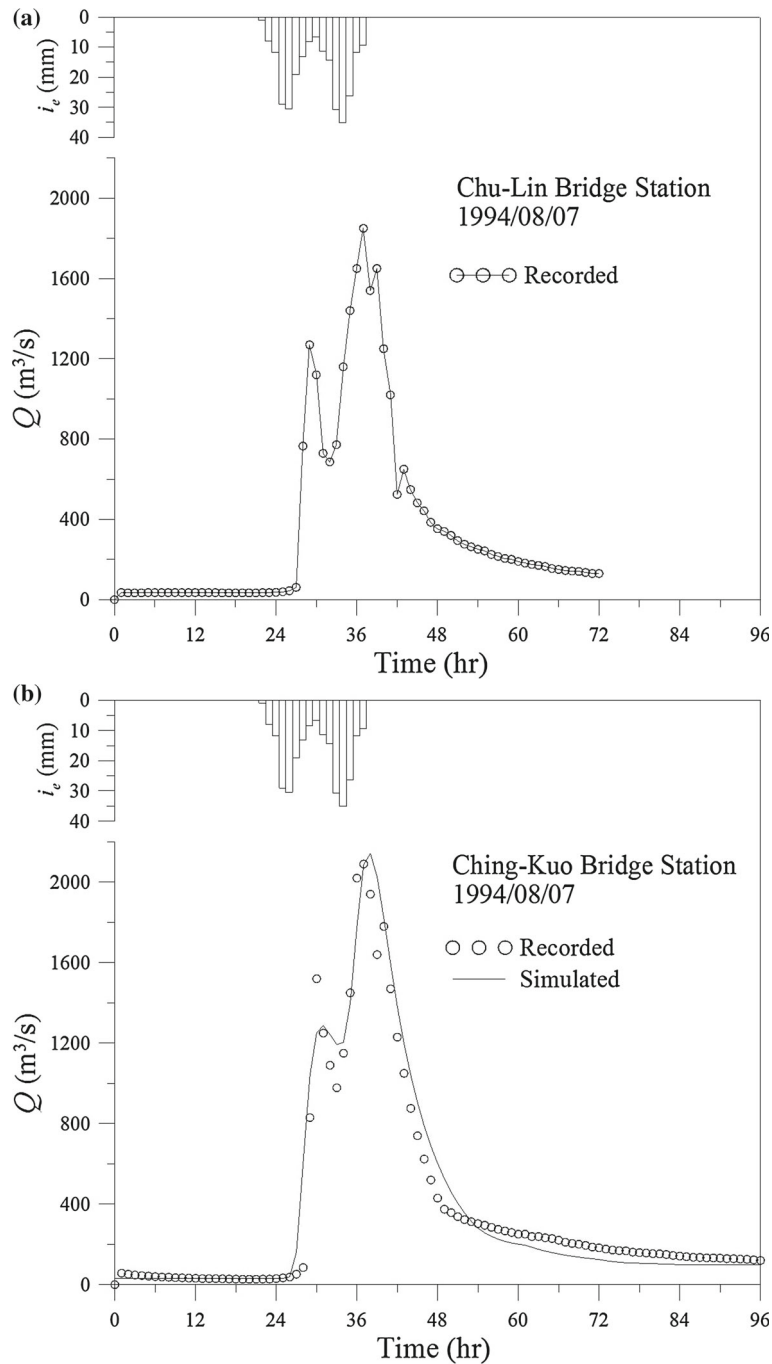


Figure 6. Verification of 1D channel-flow routing model for Typhoon Doug (a) upstream inflow hydrograph at Chu-Lin Bridge and (b) simulated hydrograph at Ching-Kuo Bridge.

in accordance with 50-yr return period at the time of 1992. Hence, the protection level of the existing levee is lower than 10-yr due to the changing climate in the past 20 years. To realize possible flooding extents in high return-period storms, the inflow hydrographs shown in figure 7 and the existing levee crest were used for further simulations. Table 2 shows the simulated results of flooding extents corresponding to different return-period

floods. Due to limited length of the paper, only the inundation maps of 20-yr and 200-yr floods are provided in figure 9. In this figure, the maximum inundated water depth of each cell during the simulation process was presented. The densely populated urban areas are marked out with red lines, and the detention reaches along the riparian farmlands are marked out with green dotted lines. The results indicate that for a 20-yr flood,



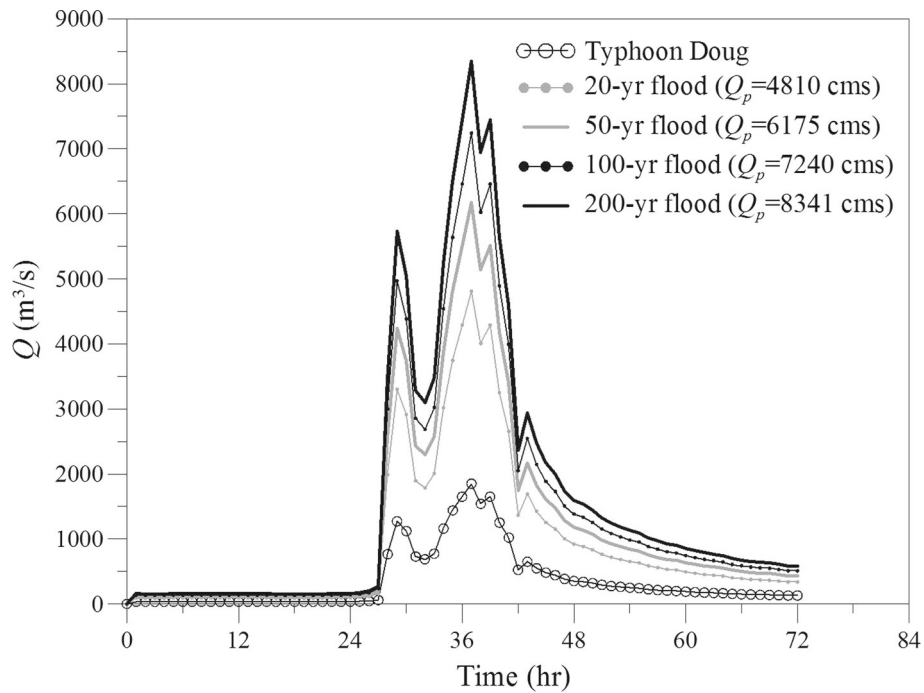


Figure 7. Designed inflow hydrographs under different return period conditions.

Table 2. Downstream flooding areas of Tou-Chien River basin under different return period conditions.

Simulation scenarios	Downstream flooding areas for different return periods (km <sup>2</sup> )			
	20-yr	50-yr	100-yr	200-yr
Applying the existing levee height	9.6	17.4	22.7	27.4
Applying the flood detention measure	0.0	2.4	4.6	7.6

Note: The inundation extents occurred in the riparian farmlands (flow detention areas) shown in figures 9 and 10 are not included for the calculation of downstream flooding areas.

a large area of inundation occurs on the left side of the river mouth. Only a small portion of urban area (red line area) on the right side of the river is inundated. However, for a 200-yr flood, severe inundation occurs on the entire estuarine area and a large portion of urban area on the right side of the river is also inundated. As listed in table 2, the downstream inundated region (without counting the flooding area occurred in the riparian farmlands) is 9.6 km<sup>2</sup> for the 20-yr flood, and the region reaches to 27.4 km<sup>2</sup> for the 200-yr flood in applying the existing levee height.

### 4.3 Flood detention assessment

Considering the changing climate to induce more frequently severe floods, heightening levees may be the most straightforward way to prevent disastrous flood hazard. However, levee heightening

or floodplain extension seems impossible in the Tou-Chien River basin because 14 bridges have been constructed along the downstream channel and a large number of buildings concentrated in the city.

Considering the topography and land use conditions in the riparian areas, two farmlands (marked out with green lines as shown in figure 5) are designated for floodwater detention. Hence, lowering the levee crest along the two farmlands is the proposed approach in this study to divert excessive floodwater from the main channel to the farmlands for temporary detention. The farmland on the left side of the river is about 9.5 km<sup>2</sup>; and the other one on the right side of the river is 12.9 km<sup>2</sup>. As shown in figure 8, the green dotted lines denote the channel reaches adjacent to the farmlands. The levees marked with green dotted lines are designated to be lowered corresponding to the

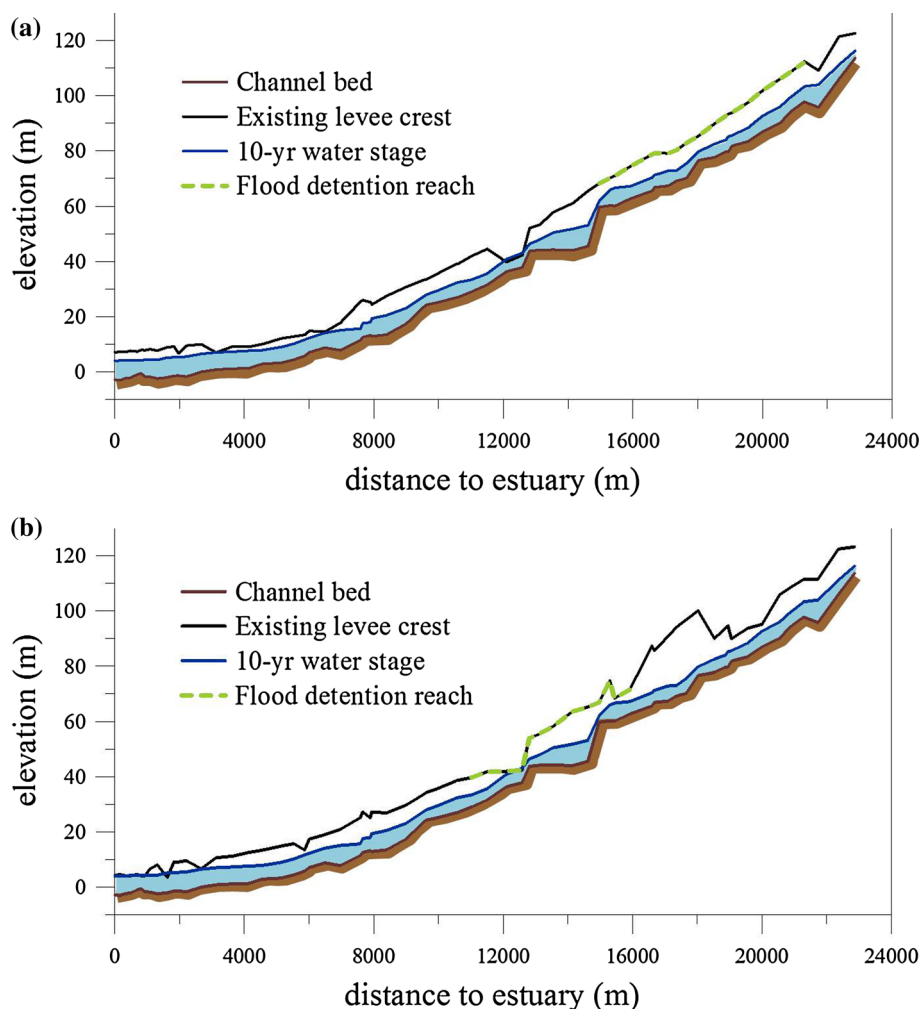


Figure 8. Longitudinal profile of channel bed and levee crest along the mainstream of the Tou-Chien River basin (a) right bank and (b) left bank.

water stage of 10-yr return-period (the blue line). Consequently, for an incoming flood larger than the 10-yr return period, part of the floodwater can be temporarily detained in the farmlands to attenuate the flood peak and to mitigate severe overbank flooding in the downstream urban areas.

Figure 10 shows the spatial distribution of inundated water depth in applying the lowered levee along the farmlands under the floods with 20-yr and 200-yr return periods. The results indicate that the proposed flood detention measure can completely prevent overbank flooding in the downstream areas for a flood event less than a 20-yr return period. For a flood larger than 20-yr return period, inundation mainly occurs near the river mouth. Nevertheless, those places currently are either rural lands or recreation parks. The flood risk can be significantly mitigated in the

densely populated urban areas (the red-line areas) even for a flood reaching 200-yr return period.

To investigate the influence of two designated farmlands on flood peak attenuation, the simulated hydrographs at section 31 (marked in figures 9 and 10) using the existing levee crest and the levee with lowered crest are compared. As shown in figures 9 and 10, section 31 is the upstream section closely adjacent to the channel reach flowing through the densely populated areas. Hence, flood peak attenuation at this section is concerned in order to mitigate the risk of urban flooding. The simulated hydrographs at section 31 and the upstream inflow hydrograph can be seen in figure 11. The solid-bold line is the hydrograph generated by applying the existing levee crest, and the hydrograph shown by bold-dashed line represents the scenario using the lowered levee in the modeling. Lower peak

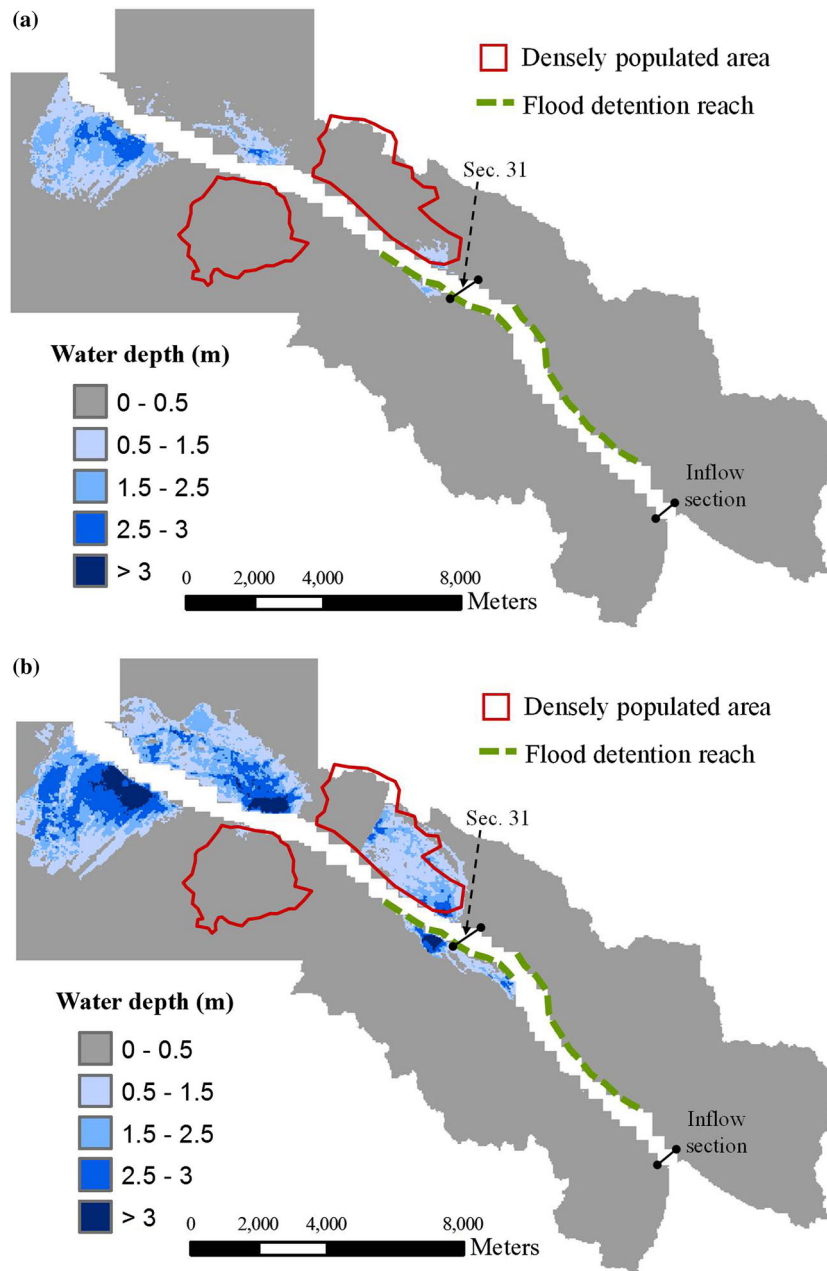


Figure 9. Comparison of flooding areas by assigning different inflow hydrographs under various return periods in applying the existing levee height for simulation. (a) 20-yr flood, existing levee height. (b) 200-yr flood, existing levee height.

discharge can be found in the simulation using the lowered-levee scenario. The flood peak at section 31 is attenuated from 4665 to 3792 m<sup>3</sup>/s for the 20-yr flood due to the flood detention in the farmlands, and the peak discharge is significantly decreased from 6534 to 3992 m<sup>3</sup>/s for the 200-yr flood.

In order to quantify the capacity of the two riparian farmlands to temporarily retain the flood water, a simple formulation was established to calculate the storage of flood water in the detention

areas as follows:

$$S_t = S_{t-1} + \left( \int I_t dt - \int O_t dt \right) \quad (8)$$

in which  $S_t$  is the storage volume retained in the farmlands at time  $t$ ;  $\int I_t dt$  is the total volume of channel flow overflowing into the farmlands through the detention reaches at time  $t$ ;  $\int O_t dt$  is the total volume of overland flow draining to the channel through the detention reaches

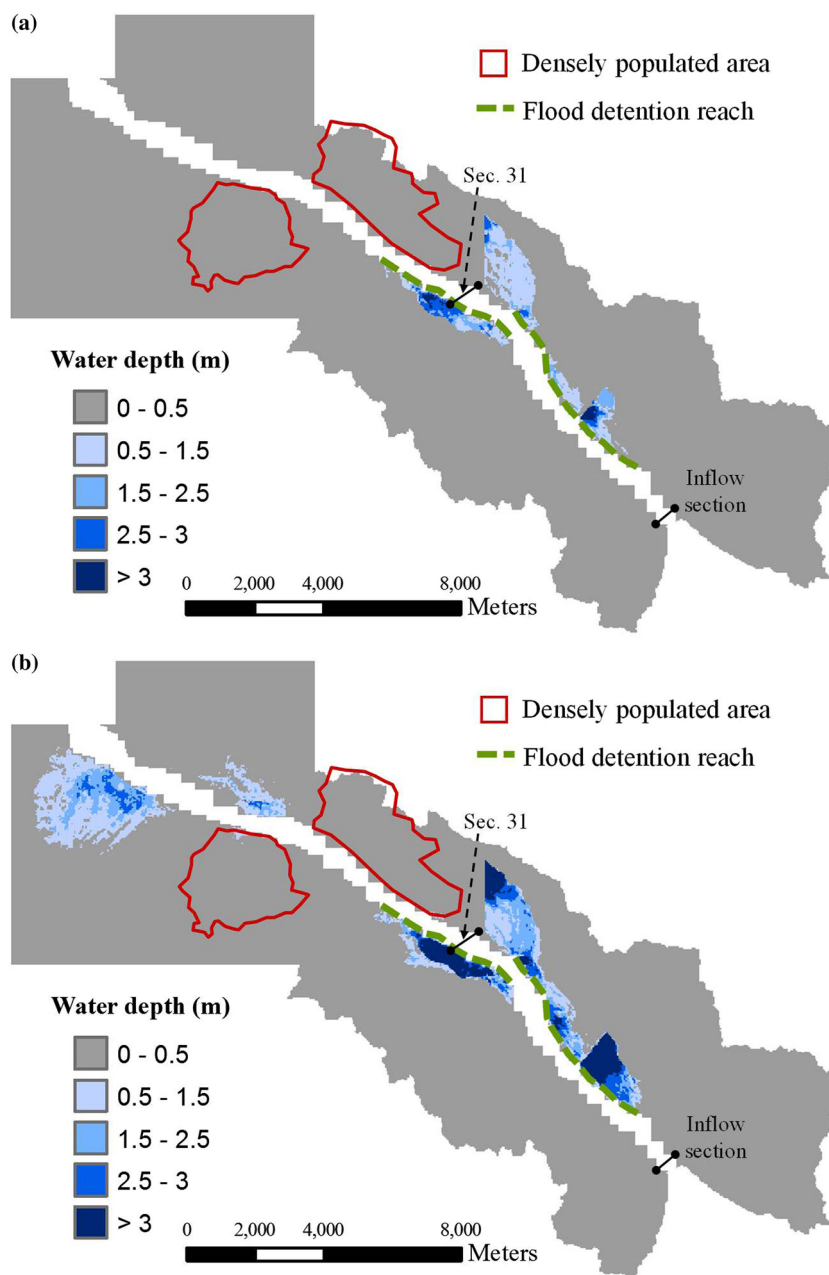


Figure 10. Comparison of flooding areas by assigning different inflow hydrographs under various return periods in applying the flood detention measure for simulation. (a) 20-yr flood, lowered levee in detention reach. (b) 200-yr flood, lowered levee in detention reach.

at time  $t$ . In this study, the flow volume diverted through the detention (marked out with green dotted lines in figures 9 and 10) was accumulated at each time step to obtain the storage volume. Figure 12 shows the storage hydrographs of the riparian farmlands during the simulation applying the proposed flood detention measure. For a 20-yr return-period flood, the maximum storage volume is about 16.4 million cubic meters. The maximum storage volume can reach to 101.5 million cubic meters for a 200-yr return-period flood,

and the storage begins to recess after 28.5 hr of the simulation (as shown in figure 12) as the volume of the detained water draining back to the channel ( $\int O_t dt$ ) exceeds the volume of channel flow overflowing to farmlands ( $\int I_t dt$ ).

To clearly evaluate the performance of the proposed measure for flood mitigation, the downstream simulated inundation areas caused by floods of different return periods are summarized in figure 13. The downstream flooding areas are estimated by accumulating the blue regions shown

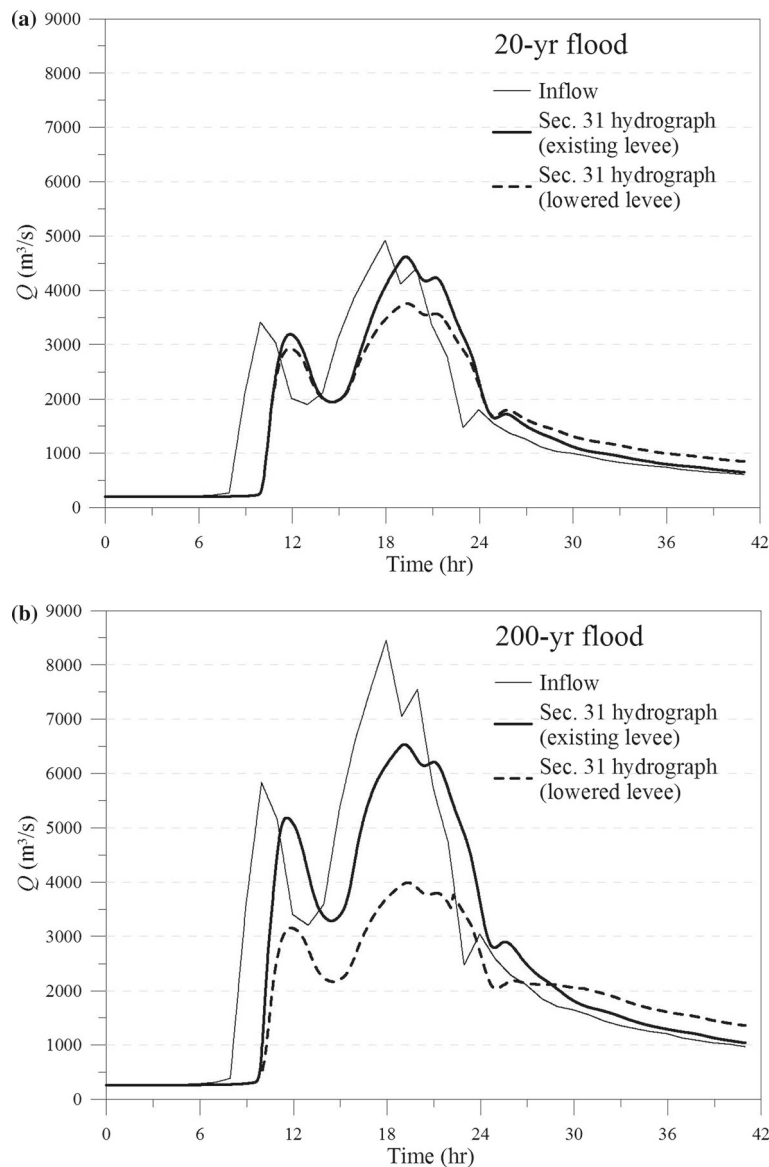


Figure 11. Flow hydrograph analysis at section 31 for the existing levee crest and lowered levee crest cases. (a) 20-yr flood and (b) 200-yr flood.

in figures 9 and 10, but not including those in the two farmlands. Figure 13 shows that the proposed detention measure can effectively mitigate downstream flooding for a 20-yr return-period flood, which would have led to the downstream inundation of 9.6 km<sup>2</sup> under the existing levee height. For a 200-yr return-period flood, the downstream inundation area is diminished from 27.4 to 7.6 km<sup>2</sup> by virtue of the flood detention measure. Although the downstream flooding cannot be completely prevented, the inundation risk in the densely populated urban areas can be greatly relieved. The comparison of downstream flooding areas between the two scenarios with different return periods of flood is also listed in table 2.

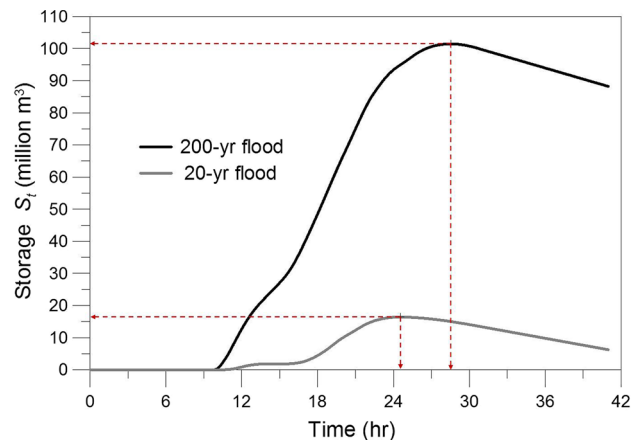


Figure 12. Storage hydrographs of the riparian farmlands during the simulation in applying the flood detention measure for different return periods of floods.

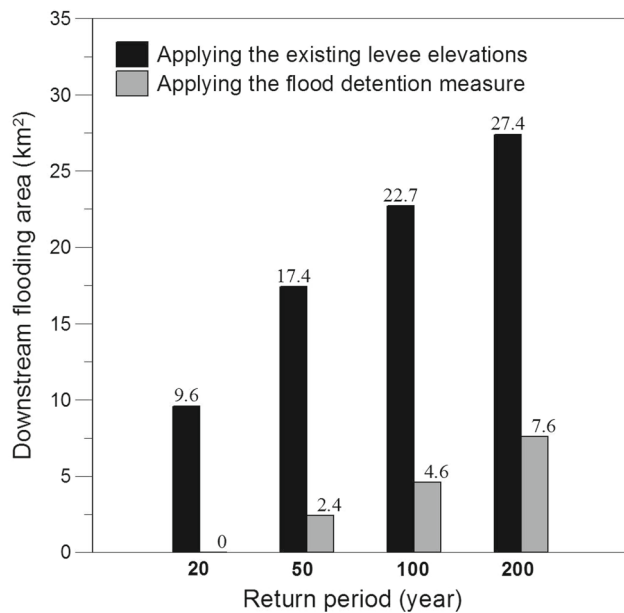


Figure 13. Comparison of downstream flooding areas in applying the existing levee and the flood detention measure for different return periods of floods.

## 5. Conclusions

As the changing climate has intensified flood hazards in Taiwan during recent years, proposing feasible plans for flood mitigation is required. According to the result of trend analysis, the flow records collected from Tou-Chien River basin shows an increasing trend in the period of 1994–2011. For this reason, the efficacy of the existing levees, which were built before 1992, need to be reevaluated. The 1D–2D flow simulation results indicated that the existing levees cannot prevent the flooding in the densely populated urban areas for a flood event higher than 20-yr return period. Therefore, diverting floodwater to upstream riparian farmlands was proposed in this study by taking advantage of the inherent topographic conditions of the basin. A series of numerical simulations showed that the flood detention measure is capable of inhibiting downstream overbank flooding for a 20-yr flood and effectively reducing downstream flooding area from 27.4 to 7.6 km<sup>2</sup> for a 200-yr flood. Although the downstream flooding cannot be completely relieved when the proposed strategy was implemented, flood inundation would merely occur in the downstream paddy fields or recreation parks instead of invading the densely populated urban areas.

## Acknowledgements

This research was supported by the Council of Agriculture and the National Science Council, Taiwan, ROC, under grants CA 080205b116 and NSC 103-2923-E-019-001-MY3. Financial support from the Council of Agriculture and National Science Council is gratefully acknowledged.

## References

- Cunge J A, Holly F M and Verwey A 1980 *Practical Aspects of Computational River Hydraulics*; Pitman Publishing Ltd., London.
- Gonwa W S and Kavvas M L 1986 A modified diffusion wave equation for flood propagation in trapezoidal channels; *J. Hydrol.* **83** 119–136.
- Hager W 1987 Lateral outflow over side weirs; *J. Hydrol. Eng.* **113** 491–504.
- Hydrologic Engineering Center 2000 *Hydrologic Modeling System: User's Manual*; U.S. Army Corps of Engineers, Davis, CA.
- Huang P C and Lee K T 2013 An efficient method for DEM-based overland flow routing; *J. Hydrol.* **489** 238–245.
- Huang P C and Lee K T 2017 Efficient DEM-based overland flow routing using integrated recursive algorithms; *Hydrol. Process.* **31** 1007–1017.
- Jain M K and Singh V P 2005 DEM-based modeling of surface runoff using diffusion wave equation; *J. Hydrol.* **302** 107–126.
- Kendall M G 1975 *Rank Correlation Methods*; Charles Griffin, London.
- Léonard J, Perrier E and Rajot J L 2004 Biological macropores effect on runoff and infiltration: A combined experimental and modelling approach; *Agric. Ecosyst. Environ.* **104** 277–285.
- Mann H B 1945 Non-parametric tests against trend; *Econometrica* **13** 245–259.
- MacCormack R W 1982 A numerical method for solving the equations of compressible viscous flow; *AIAA J.* **20(9)** 1275–1281.
- Nicholas A P and Walling D E 1997 Modelling flood hydraulics and overbank deposition on river floodplains; *Earth Surf. Process. Landf.* **22** 59–77.
- O'Callaghan J F and Mark D M 1984 The extraction of drainage networks from digital elevation data; *Comput. Vision, Graphics Image Process.* **28** 323–344.
- Ogden F L and Julien P Y 1993 Runoff sensitivity to temporal and spatial rainfall variability at runoff plane and small basin scales; *Water Resour. Res.* **29** 2589–2597.
- Pantelakis D, Zissis T, Anastasiadou-Partheniou E and Baltas E 2012 Numerical models for the simulation of overland flow in fields within surface irrigation systems; *Water Resour. Manag.* **26** 1217–1229.
- Pasche E and Rouvé G 1985 Overbank flow with vegetatively roughened flood plains; *J. Hydrol. Eng.* **111** 1262–1278.
- Ponce V M, Li R M and Simons D B 1978 Applicability of kinematic and diffusion models; *J. Hydraul. Div.* **104** 353–360.

- Preissmann A 1961 *Propagation of translatory waves in channels and rivers*; First Congress of the French Association for Computation, pp. 433–442.
- Sen Z 2012 Innovative trend analysis methodology; *J. Hydrol. Eng.* **17** 1042–1046.
- Su S H, Kuo H C, Hsu L H and Yang Y T 2012 Temporal and spatial characteristics of typhoon extreme rainfall in Taiwan; *J. Meteorol. Soc. Japan* **90** 721–736.
- Wang M and Hjelmfet A T 1998 DEM based overland flow routing model; *J. Hydrol. Eng.* **3** 1–8.
- World Bank 2005 *Natural Disaster Hotspots: A Global Risk Analysis*; World Bank Group, Washington, DC.
- Water Resources Planning Institute 2011 *The Integrated Regulation Planning of Tou-Chien River Basin*; Water Resources Agency, Ministry of Economic Affairs, Taiwan.

Corresponding editor: RAJIB MAITY